APP-ENABLED WIRELESS LOOP RESISTANCE TESTING FOR EFFICIENT EVALUATION OF AGRICULTURAL POWER SYSTEM EQUIPMENT

/

基于 APP 的无线回路电阻测试实现农业电力系统设备的高效评估

Yue YAO, Yanquan HOU*, Wei LI, Juntao ZHAO, Chen HUANG, Cen LI

State Grid Heilongjiang Electric Power Co., Ltd. Qitaihe Power Supply Company / P.R.China

Tel: +8613398601690; E-mail: 965660634@qq.com

Corresponding author: Yanquan Hou

DOI: https://doi.org/10.35633/inmateh-79-08

Keywords: *High-Voltage Switchgear; Loop Resistance Test; Abnormal Contact Resistance; Contact Wear; Agricultural power distribution network*

ABSTRACT

Agricultural power networks accelerate contact wear and reduce the accuracy of conventional loop resistance testing. This study presents an APP-based wireless three-phase synchronous measurement system integrating UC3854-driven multi-stage power factor correction (0–100 A, 82–83.17% efficiency, PF 0.99) and a supercapacitor pulse module (16 V trigger, 230 V charge). The system achieves 0.01 μΩ resolution and >10,000 MΩ insulation resistance. Field validation on 110 kV GIS reduced wiring and testing times by 67% (≤1% deviation), while 500 kV GIL measurements improved efficiency by 80%. The platform enables high-current stability, strong interference immunity, and digitalized operation.

摘要

农业配电网运行于潮湿、多尘、腐蚀性环境，加速接触磨损并降低传统回路电阻测试仪的精度。本研究开发了一种基于 APP 的无线三相同步回路电阻测试系统，采用基于 UC3854 的多级功率因数校正架构（0–100 A 恒流输出，效率 82–83.17%，功率因数 0.99）和超级电容脉冲放电模块（16 V 触发，230 V 充电）。系统实现 0.01 μΩ 测量分辨率和>10,000 MΩ 绝缘电阻，优于商用回路电阻测试仪典型的 0.1 μΩ 分辨率。现场测试表明：110 kV GIS 设备接线时间由 30 min 缩短至 10 min，测量时间由 3 min 缩短至 1 min（效率提升 67%，偏差≤1%）；500 kV GIL 区段（1.2 km）将传统五段测试整合为单次连续测量（效率提升 80%）。该系统为高电流稳定输出、强抗干扰、快速接线和数字化管理的农业配电网提供了高效可靠的测试解决方案。

INTRODUCTION

The rural power distribution network is a critical infrastructure in modern agriculture, supporting not only livestock production, irrigation systems, and primary processing, but also the integration of distributed energy and agricultural IoT. Consequently, the reliability of high-voltage switchgear—responsible for circuit control and protection—has become a key determinant of grid security (*Li, 2022*). Compared with urban systems, rural equipment is more exposed to humidity, dust, corrosive gases, and temperature fluctuations, which accelerate contact degradation and increase the risk of abnormal loop resistance, potentially leading to overheating, protection failure, and system outages (*Li et al, 2022*). Loop resistance measurement is widely used to evaluate the operational condition of GIS and GIL switchgear. According to standards such as GB 50150 and DL/T 596, resistance values should not exceed 120% of factory references, and significant phase deviations indicate potential faults. However, conventional testers face substantial limitations in rural applications. Fixed-spacing clamps often fail to meet GB/T 3048.4–2007 requirements, especially for large or irregular conductors, resulting in poor measurement reliability (*Ma et al., 2022; Deng, 2021*). Temperature variations introduce resistance drift and reduce testing efficiency due to thermal stabilization requirements *(Zhang et al., 2021*). In addition, strong electromagnetic interference in substations distorts measurement signals (*Fang, 2020; Fang, 2020b*), while traditional instruments lack real-time data transmission capabilities, hindering digital management (*Wu & Zhang, 2020*). Condition-based maintenance (CBM) has been extensively studied worldwide.

Early work by EPRI in the 1970s introduced reliability-centered maintenance concepts (*Yuan et al., 2020*), followed by developments in Japan and Europe emphasizing online monitoring and integrated diagnostic systems (*Wang et al., 2018; Ban et al., 2018*). In contrast, existing loop resistance testing technologies in China still rely on single-phase sequential measurement and wired control, limiting efficiency and data reliability (*Xiao et al., 2014*).

To address these challenges, this study develops a three-phase synchronous loop resistance testing system tailored for rural environments. The system integrates wireless APP-based control, a high power-factor constant-current source, supercapacitor-assisted pulse discharge, enhanced electromagnetic compatibility design, and optimized Bluetooth communication. It enables rapid deployment, high-precision measurement, and automated data management, thereby facilitating the transition toward condition-based and digitalized operation of agricultural power distribution systems.

MATERIALS AND METHODS

System Architecture of the Tester

Within this system, the overall topology presents a hierarchical structure composed sequentially of the front-end power equipment, sensor unit, data acquisition and processing module, signal-processing chain, and fault-diagnosis module. During operation, the power equipment generates current, voltage, and loop-impedance states that are first captured in real time by high-sensitivity sensors. After entering the data acquisition unit, the sensing signals are quantized and preprocessed according to the required sampling accuracy and bandwidth, followed by preliminary data structuring and anomaly elimination performed by an embedded processor. The signal-processing module applies filtering, denoising, feature decomposition, and parameter modeling to the acquired signals, enabling the dynamic characteristics and state parameters of the electrical circuit to be presented with an enhanced signal-to-noise ratio. The fault-diagnosis module identifies abnormal conditions—such as loop-resistance deviation, contact erosion, and poor contact—based on the extracted key features, and transmits the diagnostic results to the App interface via a wireless communication link, allowing maintenance personnel to monitor equipment health in real time and perform remote control and decision support.

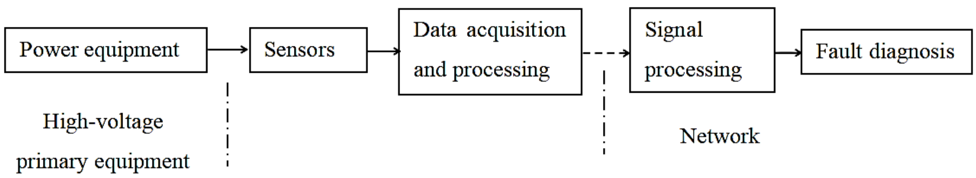

Fig. 1 – Topology of an App-Wireless-Controlled Loop-Resistance Tester for Switchgear

To eliminate the influence of temperature on the measurement results, an automatic temperature-compensation technique is employed. The ambient temperature is continuously monitored using a DHT11 temperature–humidity sensor, and the measured resistance is corrected to its equivalent value at the standard reference temperature of 20°C using the resistance–temperature conversion formula $Rt=Ro(1+\alpha t)$ (*Lai et al., 2019*). In this equation, Ro denotes the standard resistance at 20℃, Rt is the measured resistance under the current ambient temperature, and α represents the temperature coefficient of the conductor material. This correction ensures the comparability of measurement data across different environments and seasons. The main controller adopts the STM32F103C8T6, a 32-bit microcontroller operating at a clock frequency of 72 MHz, integrating a 12-bit ADC, DMA controller, and multiple communication interfaces. These features meet the requirements of three-phase data acquisition and Bluetooth communication, while its low-power operation mode supports long-duration field testing (*Chen et al., 2016*). The design schematic is shown in Figure 2.

Interference suppression is achieved through power-supply filtering, Bluetooth AFH frequency hopping, and electromagnetic-compatibility design. For GIS/GIL applications, a dedicated wireless auxiliary short-circuiting module is integrated, enabling long-distance testing within 3 km via LoRa communication. After the system is powered on, the main program performs initialization, defining system variables and assigning initial values, configuring the I/O modules, and setting parameters for the display, serial ports, and other functional modules. Once initialization is completed, the program enters a keypad-scanning routine (i.e., scanning touch-keys on the display) and responds to user operations.

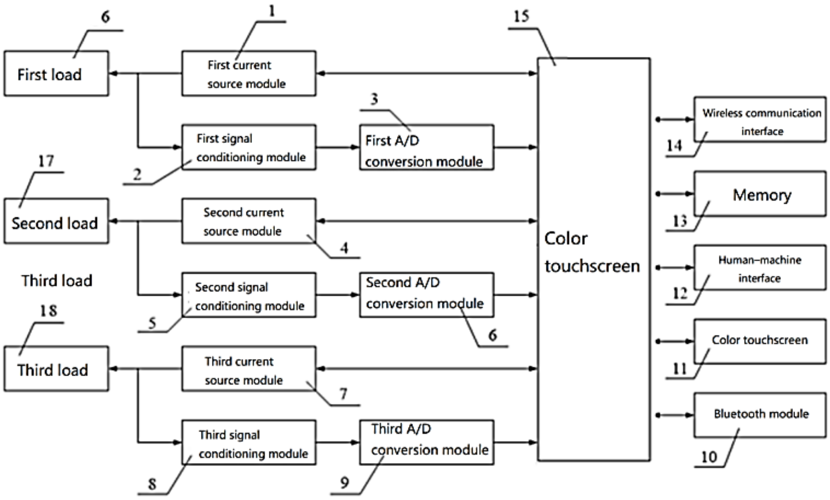

Fig. 2 – The structural schematic diagram of the tester

The GC7135B A/D converter synchronously samples three-phase current, voltage, and temperature; the STM32 computes resistance, resistivity, and temperature-corrected values transmitted to a mobile APP. The APP supports Bluetooth pairing, time sync, parameter configuration, command execution, real-time data reception, validity assessment (inter-phase deviation ≤5% as qualified), WORD report generation, and PMS interface reservation. To counter 2.4-GHz ISM band EMI (*Kusuma Neerugatti & Pakala, 2025*), a hierarchical anti-interference architecture integrates FEC, ARQ, AFH, and packet-length adaptation (*Golaghazadeh et al., 2022; Labiod et al., 2014*). Bluetooth uses 1/3-rate repetition and 2/3-rate shortened Hamming coding; ARQ with CRC enables fast retransmission via ACK/NACK (Type-I Hybrid ARQ). AFH dynamically excludes interfered channels, while variable packet lengths mitigate high-interference transmission risks. A two-tier validation framework (laboratory and field) evaluates functionality, stability, communication reliability, and applicability. Laboratory tests assess Bluetooth communication, data-display sync, constant-current output (0–100 A), measurement range/resolution, HMI, insulation, and EMC using standard resistors, calibrators, and EMI injection. Field tests on 110-kV GIS and 500-kV GIL systems (*Chen et al., 2025*) verify three-phase synchronous measurement, long-distance wireless triggering, and integrated operation; the 1.2 km GIL test validates coordinated main/remote module operation under practical grid conditions.

Development and Testing of the High-Power-Factor Power Supply

The design of the current source employs the UC3854 as the core controller to realize active power-factor correction. Based on the preset current value, the controller automatically adjusts the PWM duty ratio and regulates the switching frequency of the MOSFETs, ensuring that the output current remains stable at the specified level.

Fig. 3 – Photograph of the power supply unit

This study employs a multi-stage AC/DC/AC/DC topology with active power correction and PWM modulation for a high-power, high-power-factor intelligent DC supply (Figure 4). Module (1): rectification; (2): BOOST step-up; (3): half-bridge conversion; (4): high-frequency transformer; (5): secondary rectification; (6): temperature sensor; (7): protection unit; (8): PWM modulator; (9): UC3854-based PFC controller; (10): control interface.

Working process: Mains AC is rectified by (1) to DC bus voltage, then conditioned via the PFC loop (2, 9) to improve power factor. PWM modulator (8) drives half-bridge converter (3) to invert DC to high-frequency AC; transformer (4) provides isolation and step-down; module (5) rectifies and filters to final DC output. Temperature sensor (6) monitors power semiconductors, feeding protection unit (7) to adjust PWM (8) or activate cooling. Control interface (10) manages current setting and display. UC3854-based PFC (9) regulates BOOST input current in-phase with voltage, pushing power factor >0.95; PFC auto-activates under heavy load and disables under light load. PWM modulator (8) serves as the core control unit, adjusting duty cycle and switching frequency per preset current from (10) to stabilize output. The multi-stage structure delivers 100 A at 10 V, exceeding 500 A at 5 V.

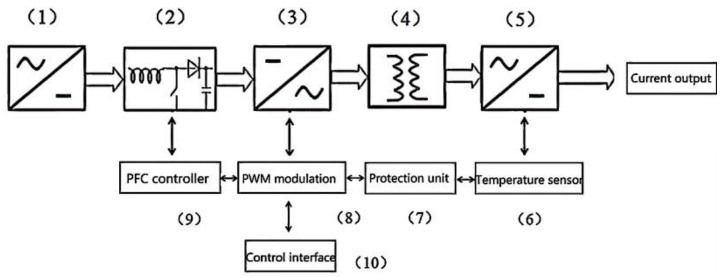

Fig. 4 – Block diagram of the current source principle

In this design, the UC3854 integrated circuit, produced by Texas Instruments for active power factor correction (APFC), is adopted. By incorporating input-voltage feed-forward technology together with the internal multiplier and divider, the loop gain of the control circuitry becomes independent of input-voltage fluctuations. This enables stable operation across the full input-voltage range while ensuring excellent dynamic response and load-regulation performance. The application schematic of the UC3854 is shown in Figure 5.

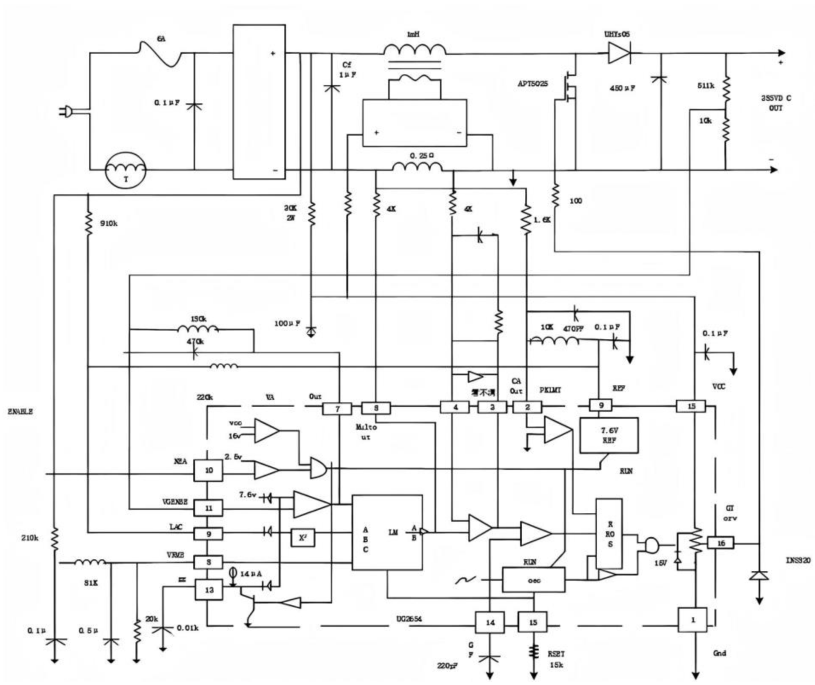

Fig. 5 – Schematic diagram of the UC3854 application circuit

Although the AC/DC and DC/AC stages provide sufficient power, the output voltage remains excessive and current capacity inadequate. A step-down transformer with rectification is therefore introduced to obtain a stable high-current DC output (*Yuan et al., 2020*). Performance evaluation focuses on efficiency, harmonics, waveform quality, thermal behavior, and electromagnetic compatibility under controlled conditions (20 ± 5 ℃, 30%–70% RH). The input is connected to a calibrated power analyzer, and the output to a programmable electronic load. Efficiency is measured from 10% to 100% load with 60 s stabilization per point. Harmonic spectra and total harmonic distortion (THD) are measured under full-load conditions, while waveform distortion, ripple characteristics, and dynamic response are evaluated using high-bandwidth oscilloscopic measurements.

Thermal performance is assessed 60 min full-load operation using thermocouples or infrared imaging to determine steady-state distribution. Electromagnetic compatibility is verified through EFT, surge, and ESD tests applied to power and signal ports, with continuous monitoring of system stability. This framework enables systematic validation of key metrics and supports subsequent system optimization.

Design of the Test Power Supply Based on Supercapacitors

Supercapacitors provide rapid charge–discharge, high power density, long cycle life (>500,000), and wide-temperature operation (−40 to 70 °C). Compared with batteries and electrolytic capacitors, they offer 30–40× higher capacitance at equal volume, faster charging (~95% within 10 s), lower ESR, and significantly enhanced instantaneous power capability. These properties enable high-current pulse generation for loop-resistance measurement. Peak current and duration depend on initial voltage U, capacitance C, inductance L, and resistance R. Large parasitic inductance induces voltage spikes, mitigated by series inductance (validated by simulation). Peak current scales with voltage, exceeding kA levels above 16 V (~2200 A at 32 V), while higher voltage or capacitance extends pulse duration. The discharge path is modeled as a series RLC circuit. Based on the zero-input response of a second-order system, pulse current generation is realized. The 220 V AC input is isolated and half-wave rectified. A microcontroller controls relay-based charging and SCR-based discharging, with a diode preventing reverse current. Charging and discharging are coordinated via optocoupler-driven switching. Experimental validation employs C=1500μF, L=15mH, shunt 100 A/45 mV, and R=0.5Ω, confirming feasibility of the proposed design.

Research on Anti-Strong-Electric-Field and Anti-Strong-Magnetic-Field Interference Techniques

Testing equipment relies on microelectronic components (ICs, digital circuits) for control, signal transmission, measurement, monitoring, and diagnostics, making it highly sensitive to transient disturbances and substation electromagnetic environments. EMC tests are essential to ensure sufficient immunity and reliable operation of intelligent high-voltage devices (*Zhang et al., 2021*). Laboratory analysis of electromagnetic environments guides controlled EMC testing to guarantee field reliability under complex scenarios. This study incorporates strong electric and magnetic field interference considerations into enclosure, high-current power source, functional/signal/communication port designs for robust field usability. For the high-current power source, differential-mode (L1) and common-mode (L3, C2, C3) filters mitigate interference from switching operations, pump start/stop transients, and transformer excitation in agricultural grids. X-class capacitor C1 (phase-neutral) provides high-frequency discharge during voltage spikes to suppress differential-mode noise coupling. Common-mode choke L3 with symmetrically arranged Y-class capacitors C2 and C3 attenuates common-mode interference from lightning, capacitor switching, and long-line transients. The combined filters ensure stable input under weak grids, long transmission lines, and strong interference, providing clean front-end power for subsequent rectification and constant-current output.

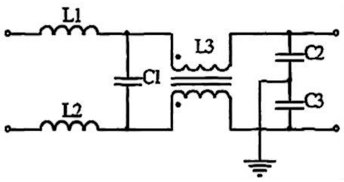

Fig. 6 – Input-End Filter Circuit of the Power Supply

An active PFC circuit at the front-end rectification stage synchronizes input current with grid voltage, maintaining near-sinusoidal waveforms to suppress harmonic injection and high-frequency distortion—critical in rural/agricultural grids where complex loads, voltage fluctuations, and high line impedance cause low-order harmonics, current distortion, sampling noise, ADC instability, and control-loop oscillations. The PFC stage stabilizes energy input, reduces conducted interference, and prevents high-frequency noise from propagating into the filter network and constant-current module. RC snubber networks across MOSFETs and IGBTs attenuate high dv/dt transients and voltage spikes, mitigating reverse voltage ringing and parasitic oscillations in inductive agricultural grid environments. This reduces radiated and conducted EMI while protecting sensors, amplifiers, and microcontrollers. A hybrid single-point and low-impedance grounding strategy minimizes grounding inductance/impedance, rapidly diverting high-frequency currents during transients to limit internal noise propagation. Critical components (drivers, communication modules, ADC units) are protected via localized shielding combined with low-impedance grounding, ensuring interference currents discharge preferentially through the shielding structure—enhancing system robustness against electromagnetic disturbances in harsh agricultural conditions.

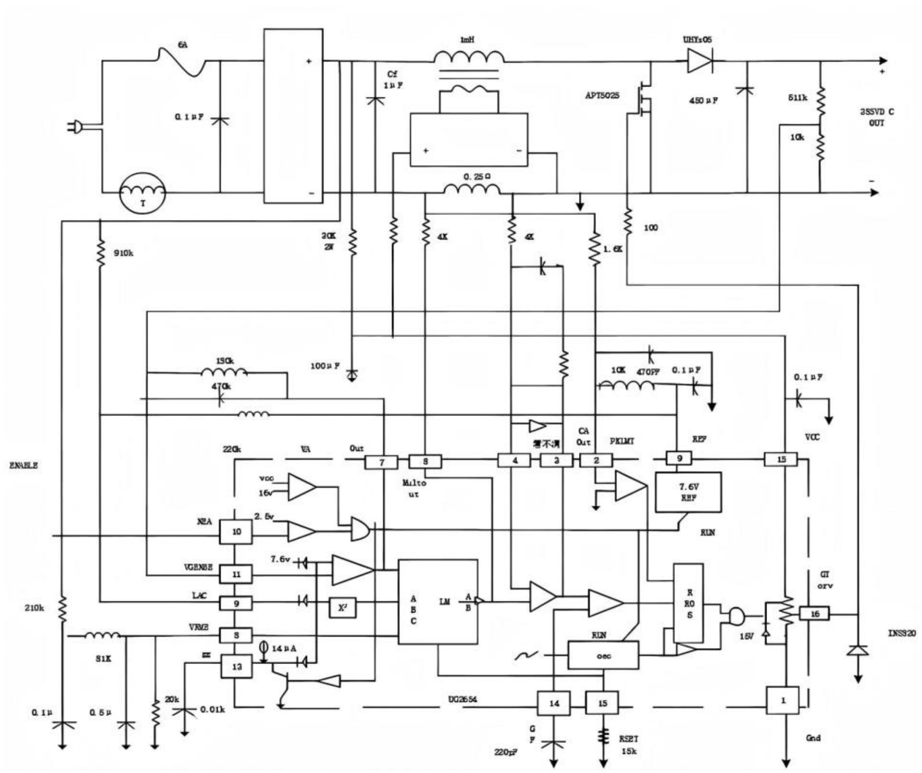

Fig. 7 – Schematic diagram of the UC3854 application circuit

Following the initial design, the AC/DC–DC/AC stages provide sufficient power but yield excessively high voltage and insufficient current capacity. To meet system requirements, a step-down transformer combined with rectification is introduced to generate a stable high-current DC output. Performance evaluation of the high-power-factor supply targets five key metrics: efficiency, harmonic characteristics, waveform quality, thermal behavior, and electromagnetic compatibility, all conducted under controlled conditions (20 ± 5 ℃, 30%–70% RH) using calibrated instrumentation. Efficiency is assessed across 10%–100% load with 60 s steady-state measurements to derive efficiency curves, while harmonic performance is evaluated at full load to obtain spectral distribution and total harmonic distortion. Waveform characteristics are captured via high-bandwidth oscilloscopic sampling to analyze distortion, ripple, and dynamic response. Thermal performance is determined through a 60 min full-load test, with temperature evolution monitored at critical components to establish steady-state distribution. Electromagnetic compatibility is verified by applying EFT, surge, and ESD disturbances to power, enclosure, and signal ports, while continuously tracking system stability and measurement integrity. This unified framework ensures systematic validation of electrical, thermal, and anti-interference performance, providing a robust basis for subsequent optimization and system integration.

RESULTS

Performance Testing of the High Power Factor Power Supply

To satisfy on-site testing requirements in rural grids, the high power factor DC supply was experimentally validated across 10%–100% load conditions. The efficiency curve demonstrates that, despite minor fluctuations at low load due to unstable grid quality, efficiency stabilizes beyond 40% load and exceeds 82% at full load, with a peak of 83.17%. This ensures stable current delivery under intermittent agricultural loads and enhances the consistency of loop resistance measurements. Harmonic analysis under full-load conditions shows low total harmonic distortion with a dominant fundamental component, confirming that the PFC design effectively suppresses harmonic amplification in weak rural distribution networks, thereby preventing measurement instability caused by harmonic interference. Thermal testing indicates that after 60 min full-load operation, key components stabilize at 113 °C (transformer) and 117–118 °C (rectifier), remaining within safe limits under a 23°C ambient environment and demonstrating suitability for prolonged field operation. Electromagnetic compatibility results further reveal that, under EFT, ESD, and RF disturbances typical of rural grids, the system maintains stable output without data interruption or fluctuation. Overall, the proposed power module exhibits high efficiency, thermal reliability, and strong anti-interference capability, providing a robust energy foundation for three-phase high-current loop resistance testing.

Table 1

Values under different load conditions

	Efficiency test value 220 Vac -50 Hz	**Target efficiency value**	**Conclusion**
Efficiency at 20% load	93.20%	>82%	Through
Efficiency at 50% load	94.30%	>85%	
Efficiency at 100% load	92.80%	>82%	
Power factor at 100% load	0.991	>0.9	

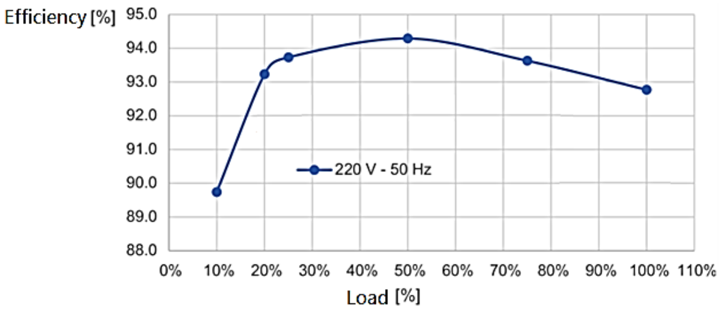

Fig. 8 – Efficiency curve under different load conditions

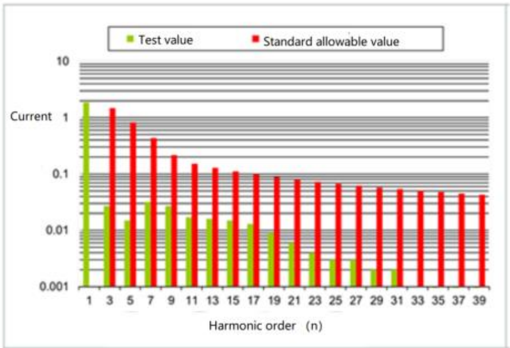

Fig. 9 – Harmonics under full-load conditions

Fig. 10 – Voltage and current waveforms

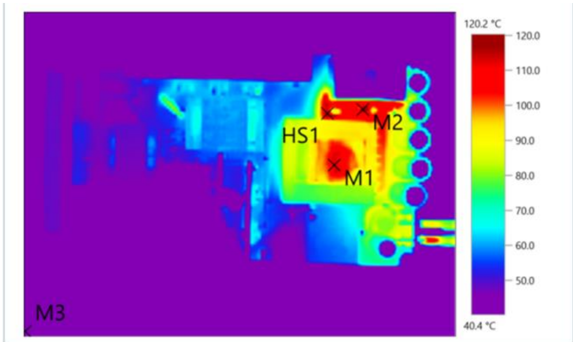

Fig. 11 – Temperature measurements

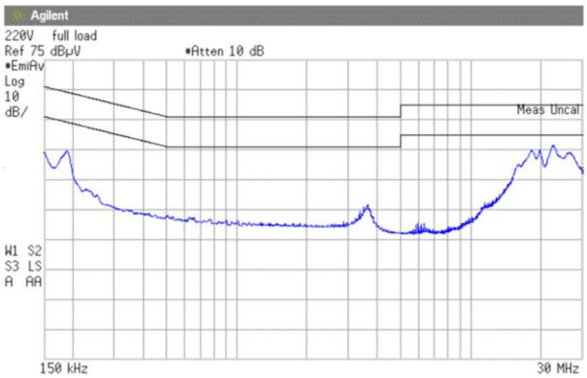

Fig. 12 – Electromagnetic compatibility (EMC) testing under full-load conditions

Supercapacitor Performance Testing

Figure 13 presents the supercapacitor discharge waveform at (U=16\text{ V}), where the current rapidly reaches its peak with a smooth rising edge and no observable spike interference, confirming that the current-limiting inductor and conduction control effectively suppress inductive transient distortion typical of rural grids. When the capacitor bank is charged to 230 V, the output current stabilizes at 100 A and remains steady throughout discharge without collapse induced by line inductance, contact instability, or humidity variations, demonstrating its capability to provide a reliable pulse source for high-impedance test circuits.

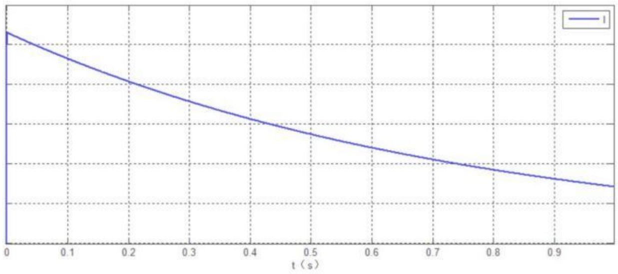

Fig. 13 – Discharge Current Waveform of the Supercapacitor at a Charging Voltage of U = 16

Figure 14 further exhibits an underdamped RLC response with low oscillation amplitude and smooth decay, indicating proper impedance matching. Compared with conventional capacitor discharge, which often produces voltage spikes and abrupt current transitions under humid and variable-temperature conditions, the proposed design suppresses initial peaks via series inductance, ensuring stable loop current and preventing false triggering of protection mechanisms. These results collectively confirm that the supercapacitor-based power supply offers high stability, reliability, and environmental adaptability, making it well-suited for deployment in rural distributed power testing scenarios.

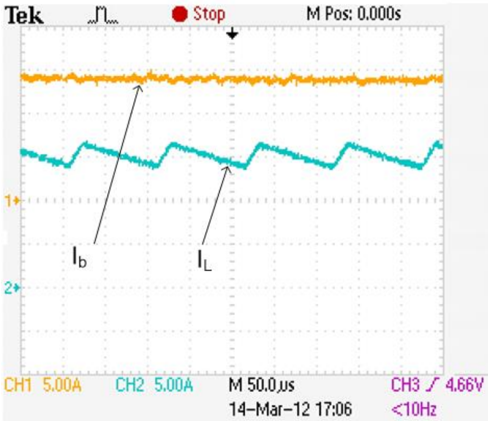

Fig. 14 – Discharge Current Waveform of the RLC Circuit

Performance Testing of the Tester

Comprehensive performance evaluation, conducted in accordance with technical specifications, confirms that the system fulfills all critical functional and operational requirements. Stable Bluetooth communication and WORD-format report export compatible with PMS platforms are achieved. The system provides real-time display of resistance, voltage, current, resistivity, and temperature-corrected values with design-level precision. The DC constant current source operates within 0–100 A, ensuring smooth regulation without overshoot. Measurement range covers 0–19,999 μΩ with 0.01 μΩ resolution, meeting micro-ohm accuracy demands. The human–machine interface integrates a 7-inch 800×480 touchscreen and high-speed thermal printing for rapid reporting. Insulation resistance exceeds 10,000 MΩ, far above the ≥0.5 MΩ requirement. Under full-load conditions (100 A), stable multi-module operation is maintained, with power conversion efficiency ≥82% and power factor up to 0.99 (GB/T14549-93 compliant). Electromagnetic compatibility testing further verifies that all ports satisfy immunity requirements, with no functional degradation or data distortion observed.

Table 2

Test Report Indicators

Testing Item	Technical Requirement	Test Result
Bluetooth Functionality	Must be able to upload data, export data documents, control data acquisition, and generate documents; meet PMS system requirements for document format and data.	Successfully uploads data, exports documents, allows control and generation of documents, meeting PMS system format and data requirements.
Data Display	Must display resistance, voltage, current, resistivity, and resistance values at standard temperature.	Successfully displays resistance, voltage, current, resistivity, and resistance values at standard temperature.

Testing Item	Technical Requirement	Test Result
DC Constant Current Source	Must output 0–100 A test current, with built-in stepwise current increase function.	Outputs 0–100 A test current with stable stepwise increase.
Measurement Range & Resolution	Range: 0–19,999 μΩ; Resolution: 0.01 μΩ	Range: 0–19,999 μΩ; Resolution: 0.01 μΩ
Human–Machine Interface	Equipped with 800×480 HD color 7-inch touchscreen for user interaction.	Equipped with 800×480 HD color 7-inch touchscreen, fully operational.
Insulation Performance	Insulation resistance between instrument casing or panel and ground must be ≥0.5 MΩ.	Measured >10,000 MΩ, far exceeding requirement.

Field tests were conducted on 110 kV GIS equipment at a 220 kV substation in Liaoning Province. The results demonstrate the following advantages of the proposed method:

Connection Efficiency: Simultaneous three-phase connection reduced the setup time from 30 min, required for conventional sequential single-phase connection, to 10 min, representing a 67% improvement.

Testing Duration: Simultaneous three-phase testing completed the full testing procedure within 1 min, compared with 3 min for conventional sequential testing, resulting in a further 67% reduction in testing time.

Data Reliability: The measured phase resistances were 35.95 μΩ (phase A), 36.04 μΩ (phase B), and 35.61 μΩ (phase C). The inter-phase deviation was less than 1%, satisfying the qualification criteria, while the deviation from laboratory-calibrated reference values remained within 0.5%, demonstrating higher accuracy than conventional testing instruments.

For 500 kV GIL testing over a distance of 1.2 km, a wireless auxiliary short-circuit device was coordinated with the main testing unit. Conventional segmented measurement, requiring five segments and approximately 5 min of total testing time, was replaced by single-connection testing completed within 1 min, corresponding to an 80% improvement in testing efficiency. The measured loop resistance was 72.5 μΩ, with a deviation of less than 1% compared with the conventional measurement result of 73.1 μΩ, thereby verifying the accuracy of long-distance testing.

Fig. 15 – Field measurement image of the loop resistance tester

CONCLUSIONS

This study develops a high-power constant-current source based on an AC/DC/AC/DC multi-stage architecture integrated with a UC3854 PFC circuit, achieving a power factor of 0.99 and efficiency above 82% under full load, while maintaining stable output in rural grid conditions characterized by voltage fluctuation and harmonic disturbance. Coupled with an RLC-optimized supercapacitor pulse module, the system delivers smooth, controllable high-current waveforms, ensuring stable excitation even in high-impedance and high-inductance loops, thereby overcoming current collapse issues and improving measurement repeatability. To ensure operational reliability, a comprehensive electromagnetic compatibility framework is established, incorporating differential/common-mode filtering, PFC shaping, RC snubber circuits, single-point grounding, and shielding structures. Experimental validation confirms stable performance in communication, data acquisition, and micro-ohm-level measurement without data drift under EFT, ESD, and RF interference, demonstrating strong anti-interference capability. Field applications further verify system effectiveness.

In 110 kV GIS testing, connection and measurement times are reduced by 67%, while in 500 kV GIL systems, integrated wireless testing improves efficiency by 80%. Across all scenarios, phase deviation remains below 1% and measurement error within 0.5%, confirming high consistency and reliability. Overall, the proposed APP-based wireless three-phase synchronous loop resistance testing system integrates high-efficiency power supply, supercapacitor pulse discharge, and robust EMC design to achieve accurate, efficient, and reliable testing in rural power grids, providing a practical solution for condition monitoring and digitalized operation of agricultural distribution systems.

ACKNOWLEDGEMENT

This work is supported by the Science and Technology Project of State Grid Heilongjiang Electric Power Co., Ltd (The Research and Application Circuit Resistance Testing Method of Switch Equipment Based on wireless synchronization)(522424250002).

REFERENCES

[1] Ban, L., Zheng, B., Zhou, P., Han, B., Xiang, Z., Sun, G., Wang, X., Wang, D., Liu, B., Teng, W., & Liu, Y. (2018). Research and engineering application of phase selection closing technology for UHV AC transformers. *Power System Technology*, 42(04), 1226–1233.

[2] Chen, J., Dong, J., & Zhao, Y. (2016). Analysis of GIS equipment conductive loop resistance testing. *Yunnan Electric Power Technology*, (S2).

[3] Chen, Y., Yan, J., Wang, Y., Wu, Y., & Liu, Z. (2025). A novel localization method for partial discharge in GIS based on electromagnetic time reversal technique. *Measurement*, 253(B), 117599. https://doi.org/10.1016/j.measurement.2025.117599

[4] Deng, M. (2021). Efficiency improvement of fixed switchgear loop resistance testing. *Journal of Chongqing College of Electric Power*, 26(06), 1–3.

[5] Fang, C. (2020). Discussion and innovation of loop resistance measurement methods. *Power Equipment Management*, (06), 181–182.

[6] Fang, H. (2020). Discussion and innovation of loop resistance testing methods. *China Electric Power Enterprise Management*, (21), 94.

[7] Gao, F. (2003). *Intelligent testing of switch loop resistance* (Master's thesis). Dalian University of Technology.

[8] Golaghazadeh, F., Coulombe, S., & Robert, J.-M. (2022). Residual packet loss rate analysis of 2-D parity forward error correction. *Signal Processing: Image Communication*, 102, 116597. https://doi.org/10.1016/j.image.2021.116597

[9] Labiod, H., Zeadally, S., & Tebchrany, E. (2014). Performance analysis of a cross-layered incremental redundancy hybrid automatic repeat request (CL IR-HARQ) mechanism. *Ad Hoc Networks*, 23, 109–120. https://doi.org/10.1016/j.adhoc.2014.06.006

[10] Lai, J., Peng, H., Jiang, Y., Hu, J., Huang, S., & Wang, W. (2019). Research on rapid GIS conductive loop resistance measurement without disassembling grounding lines. *Electric Measurement & Instrumentation*, (15), 1–6.

[11] Li, J.; Wu, X.; Chow, S.K.W.; Zhuang, Q.; Habert, G. (2023). Thermal Comfort Comparison and Cause Analysis of Low-Temperature High-Humidity Indoor Environments of Rural Houses in Gansu Province, China. *Sustainability*, 15, 16428. https://doi.org/10.3390/su152316428

[12] Li, L. (2022). Study on the measurement of conductive loop resistance of 500 kV GIS circuit breakers. *Hydropower and Pumped Storage*, 8(01), 90–93.

[13] Ma, Y., Li, X., Zhou, X., Liu, W., Ai, S., & He, N. (2022). Research on transformer excitation inrush current suppression based on high-voltage vacuum rapid circuit breakers. *High Voltage Apparatus*, 58(10), 136–142.

[14] Neerugatti, K., & Pakala, V. (2025). Design of 2.54 GHz active inductor-based LC-voltage controlled oscillator for Bluetooth/WLAN applications. *Integration*, 105, 102487. https://doi.org/10.1016/j.vlsi.2025.102487

[15] Wang, W., Wang, X., & Tang, H. (2018). Field test method of high-voltage circuit breaker loop resistance. *Electrical Technology and Economy*, (06), 27–29.

[16] Wu, H., Jiao, C., Cui, X., Liu, X., & Ji, J. (2017). Transient electromagnetic disturbance induced on the ports of intelligent component of electronic instrument transformer due to switching operations in 500 kV GIS substations. *IEEE Access*, 5, 5104–5112.

[17] Wu, Y., Yan, W., Chen, H., Zhang, W., & Ma, H. (2022). Research on interferences of VFTO to irregular distributions of secondary side cables. *IEEE Transactions on Power Delivery*. https://doi.org/10.1109/TPWRD.2022.3197318
[18] Wu, Z., & Zhang, C. (2020). Research and design of a novel loop resistance tester. *Electronic Testing*, (09), 108–109+111.
[19] Xiao, J., Wang, Y., Lü, J., & Han, W. (2014). Research on a novel circuit breaker loop resistance testing system. *Electric Measurement & Instrumentation*, 51(05), 67–72.
[20] Yuan, C., Wei, D., & Liu, K. (2020). Research on a novel circuit breaker loop resistance tester. *China New Technology & New Products*, (01), 24–26.
[21] Zhang, J., Zhen, C., Lü, B., Wei, C., Niu, L., & Ji, K. (2021). Verification method of circuit breaker breaking capacity based on final current half-wave energy. *Electrical Appliances and Energy Efficiency Management Technology*, (07), 56–60.